JOURNAL
OF THE BULGARIAN GEOGRAPHICAL SOCIETY

Accuracy assessment of high-resolution terrain data produced from UAV images georeferenced with on-board PPK positioning

Davis Dinkov

Department of Geography, National Institute of Geophysics, Geodesy and Geography – Bulgarian Academy of Sciences, Sofia, Bulgaria
* Corresponding author: davisdinkov@nauka.bg

Key words:
Direct georeferencing, DSM, HRTD, orthomosaic, point cloud, structure from motion (SfM)

ABSTRACT

In recent years, unmanned aerial vehicles (UAVs) have increased rapidly and successfully established themselves as a tool for the rapid collection of high-resolution images as baseline data in land cover studies and topographic mapping. In photogrammetry using the SfM-MVS method of processing captured images, indirect georeferencing of the digital data through ground control points (GCPs) is usually applied. But selecting, marking, and coordinating GCPs in hard-to-reach terrains is time-consuming and sometimes dangerous or impossible. The main objective of this study is to evaluate the accuracy of high-resolution topographic data (HRTD) products of photogrammetric processing of PPK-directly georeferenced images by SfM-MVS workflow. Direct and indirect methods of georeferencing digital products are compared. The planimetric and vertical root mean square error (RMSE) in the position of the validation points were calculated by the differences between measured coordinates in dense point clouds, orthophoto mosaics, and terrain surfaces (DSM), and precisely measured coordinates of the validation points by GNSS-RTK receivers. The analysis is based on a statistical evaluation of experimental data obtained from a TAROT X6-based hexacopter equipped with two different image sensor configurations: 1) Sony RX0 action camera and 2) Sony A6000 mirrorless camera, and 3) DJI Phantom 4 Pro quadcopter with integrated additional L1-GNSS module for direct georeferencing by PPK-method. HRTD generation was performed with three block control configurations for each UAV: 1) Indirect georeferencing via GCP only, 2) PPK direct georeferencing without GCP, and 3) PPK georeferencing using one GCP. Our research showed that when using L1-GNSS onboard receivers for PPK-georeferencing without any GCPs, the point cloud's planimetric accuracy (RMSExy) was from 0.125 to 0.231 cm, depending on the UAV/camera configuration. However, two flight missions produced significant vertical offsets, most likely due to ionospheric disturbances affecting the resolution of phase cycle ambiguities in the single-frequency receivers used. When adding one control point in the PPK georeferencing method, the planimetric and vertical accuracy of the data is comparable to the indirect GCP referencing method. Furthermore, our results show that camera properties (i.e., focal length, resolution, sensor quality) affect the quality and accuracy of digital products. The HRTDs were also evaluated according to the ASPRS (American Photogrammetry and Remote Sensing Society) Standards for Accuracy of Digital Geospatial Data. Analyzing the accuracy of the HRTDs obtained with the experimental UAV/camera configurations for the test area, the present study shows that the PPK-SfM-MVS workflow can provide quality data with a centimeters accuracy of the photogrammetric products.

OPEN ACCESS

Article processing
Submitted: 03 July 2022
Accepted: 04 April 2023
Published: 11 April 2023
Academic editor: Alexander Gikov

1. Introduction

Unmanned aerial systems are a successful alternative for remote sensing data collection with a wide range of practical applications. High-resolution digital topographic data (HRTD) obtained by UAV unmanned photogrammetric surveying are typically several or even below 1 cm resolution. These data can be used to map or survey landscape features that cannot be identified at low resolutions. Aerial imagery typically acquires 10–100 cm/pixel resolution, and for satellite systems, the usual publicly available data is above 50 cm/pixel resolution. In recent years, UAVs have been developed

with additional RTK/PPK GNSS systems implemented for direct georeferencing of captured imagery.

HRTDs obtained by Structure from Motion (SfM)-photogrammetry are, in the initial processing, generated in an arbitrary reference frame. Georeferencing involves transforming this initial data from an arbitrary to a predefined coordinate reference system (Harwin and Lucieer 2012). This can be done either directly using known external parameters of the photographs ("direct georeferencing") or by providing appropriate coordinates of points (ground control points or GCPs) that are recognizable on the pictures ("indirect georeferencing") (Sanz-Ablanedo et al. 2018).

The main idea is to rely entirely on direct referencing technology in the workflow without needing geodetic surveys (i.e., calculating the photogrammetric model using only image coordinates for georeferencing). Using such a simplified process would be applicable in many studies where it is difficult or impossible to place and measure ground control points (GCPs). To obtain high-resolution digital data (i.e., point clouds, orthophoto mosaics, digital surface models (DSM) or digital terrain models (DTM), the captured direct georeferenced images are processed applying Structure from Motion (SfM) - Multi-View Stereo (MVS) working photogrammetry process. SfM-MVS originates from computer vision and photogrammetry (Smith et al. 2016), requires minimally expensive equipment or expertise, and under certain conditions, can produce point clouds of comparable quality to existing survey methods (e.g., ground or airborne laser scanning). The combination of aerial photographs captured by UAV and processed by SfM-MVS workflow allows the reconstruction of three-dimensional (3D) models of surfaces based on a set of digital RGB images from different viewpoints (Eltner et al. 2016).

The application of RTK/PPK direct georeferencing by integrating an additional GNSS receiver on board the UAV is studied in the publications of (Forlani et al. 2018; Fazeli et al. 2016; Stöcker et al. 2017). A study conducted by (Zhang et al. 2019) investigated the application of the PPK-method for georeferencing, demonstrating results comparable to and better than using the indirect GCP-method. Other branches in which the application of the direct georeferencing method has been studied are: forest areas (Tomaštík et al. 2019), dam and riverbed erosion (Duró et al. 2018), landslides (Jovančević et al. 2016), coastal erosion (Harwin and Lucieer 2012; Turner et al. 2016) and others.

Most scientific research and experiments have used high-quality, more expensive dual-frequency GNSS receivers (L1/L2). With them, a fast fixed solution and precise georeferencing of the images captured by the UAV are achieved. At the same time, many UAVs are already available in which budget portable single-frequency GNSS receivers (L1) are implemented. These systems are used with single-frequency GNSS receivers for base stations. However, there is insufficient research to confirm the hypothesis of achieving centimeter accuracy in image georeferencing with single-frequency receivers. We investigated the positional and vertical accuracy of HRTDs (3D point cloud, orthophoto mosaics, and digital surface models (DSM)) generated by UAS-PPK-SfM workflow, performed flight missions with different camera/UAV configurations with integrated L1 -GNSS receivers.

The main objective of this study is to quantify the performance of the PPK–SfM-MVS framework in the context of HRTD production for the Earth's surface where centimeter accuracy is required.

2. Data and Methods

2.1. Study Area

The research experiment was carried out on forest land near the village of Plana, near the geodetic observatory of the National Institute of Geophysics, Geodesy and Geography at the Bulgarian Academy of Sciences. The test site is 36 km from the center of the capital Sofia. The area has a slope of about 4.75° from north to south, with an average altitude of 1200 m. Predominant herbaceous vegetation with coniferous forest on the periphery of the test area (Fig. 1).

2.2. Hardware equipment

2.2.1. UAVs platforms

Two flight configurations were used to conduct the experiments:

- A custom-built hexacopter based on the TAROT X6 (Fig. 2a, b) that we tested with two cameras: a) Sony A6000 – mirrorless camera with interchangeable optics (on E-mount, Exmor™ APS-C HD CMOS sensor with approximately 24.3

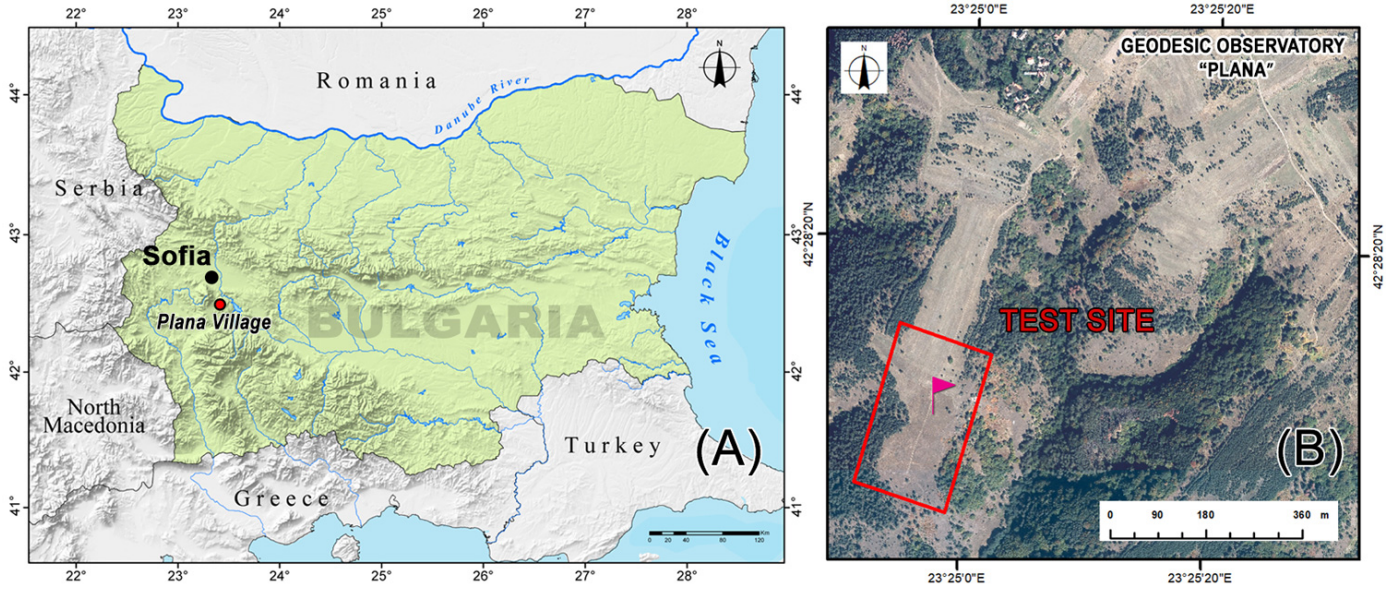

Figure 1. Study area: (A) Location of the study area within the borders of Bulgaria (42°28' N; 23°24'E); (B) Location of the test site near the Geodetic Observatory in the Plana Mountain.

effective megapixels; b) Sony RX0 – action camera (15.3Mp 1″type stacked CMOS sensor, Bionz X processor, ZEISS Tessar T lens* 24 mm f /4);

- DJI Phantom 4 Pro (P4P) – Fig. 2(c). The P4P is equipped with a DJI FC6310 camera with a nominal focal length of 8.8 mm and a 1" CMOS 20-megapixel sensor. A detailed description of the flight configurations can be found in (Dinkov 2020).

2.2.2. PPK-GNSS module

To implement the PPK-GNSS experiment, we used the platforms equipped with a single-band compact GNSS-RTK receiver (Reach M +, Emlid Ltd) with RTK / PPK capabilities and a Single-band RTK GNSS receiver with centimeter precision (Reach RS+, Emlid Ltd) as a base station. The base station is mounted on a tripod located in the outline of the test area for aerial capturing. The maximum distance between the UAV and the base station is 216 m. The base receiver is configured to log the raw data to a RINEX file at 5 Hz using GPS and GLONASS satellites. The GNSS-Rover (mounted on the UAV) records the raw GNSS data in UBX format using GPS and GLONASS satellites. The Phantom 4 antenna model is Tallysman TW2710, which covers the GPS L1, GLONASS G1, BeiDou B1, Galileo E1, and SBAS (WAAS, EGNOS, and MSAS) frequency bands. The antenna is mounted on a special plate with the center just above the center of the camera lens to minimize the offset between the antenna's phase center and the camera's projection center. The height of the antenna is 23 cm, and this difference between the projection center of the antenna and the camera is taken into account during post-processing. The Phantom 4 Pro's front LEDs flash every time a photo is taken. A phototransistor registers the blink, and the timestamp is written to the Reach m+ log file. Timestamps are extracted and combined with the photos as precise geotags.

The same GNSS single-frequency receiver is used in the Tarot X6 configuration. The UAV camera trigger "Seagull #MAP2" was used to capture the camera, which also sends a signal to the Reach M+ to record the time stamps. A Tallysman HC871 helical antenna is mounted in this configuration.

2.3. Data collection

The aerial capturing with the different flight configurations was carried out in one day in September 2020. For the subsequent evaluation of the digital products, GCPs stabilized in the test area were used, as well as additional validation points (Fig. 3).

Figure 2. UAVs platforms: (a, b) Tarot X6 hexacopter; (c) DJI Phantom 4 Pro with installed PPK-GNSS kit.

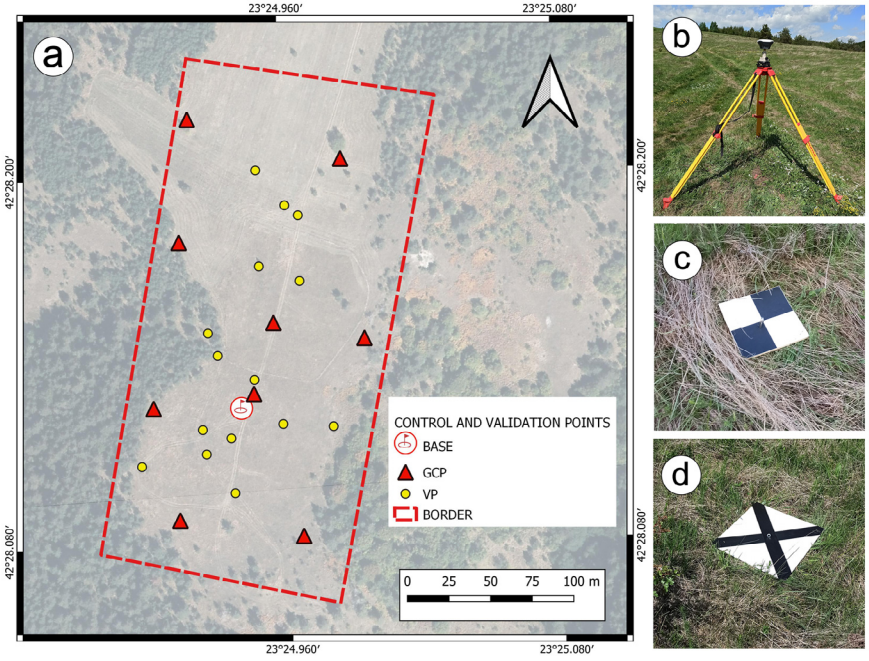

Figure 3. Control and validation points: (a) Test area with location of GCP and VP; (b) Base Station - Emlid Reach RS+; (c) Control Point (GCP); (d) Validation points.

2.3.1. Flight planning

Photogrammetric missions are predefined with the flight planning software Mission Planner (for the TAROT X6 UAV) and UgCS (SPH Engineering 2022) for the Phantom 4 Pro UAV) with the following characteristics:

1. For the TAROT X6 UAV: flight height 75 m, photos overlapping 80% and side-lap 70%, speed - 7 m/s.
2. For the Phantom 4 Pro UAV: flight height 65 m, photos overlapping 80% and side-lap 70%, speed - 5 m/s. Summary indicators for the conducted flight missions are presented in Table 1.

2.3.2. Ground control and validation points

We used 24 control and validation points distributed evenly over the test area to assess accuracy. Depending on the georeferencing method, different combinations of points were applied as control or validation.

2.4. Data Processing

2.4.1. SfM-MVS-PPK workflow with accuracy assessment

The SfM method is based on matching features (points) in multiple overlapping images to simultaneously and automatically solve the 3D camera position and image geometry (Fonstad et al. 2013). The SFM method evaluates the photo's location, orientation, and camera parameters. The MVS process uses this location and orientation (i.e., the parameters from the SFM) and computes a 3D dense point cloud. So, to produce HRTD from a set of images, one must first go through SFM and then apply MVS (Furukawa and Hernández 2015). When we use PPK direct georeferencing to the UAV images, we can call the whole workflow PPK-SfM-MVS schematically depicted in Fig. 4.

Table 1. Summary data of flight missions - September 2020

Date	UAVs	Camera	Mission number	Flight height (m)	Speed ($m\,s^{-1}$)	Estimated GSD ($cm\,px^{-1}$)
19 September 2020	Tarot X6	Sony A6000	X6.20.1	75	7	1.6
19 September 2020	Tarot X6	Sony RX0	X6.20.2	75	7	2.5
19 September 2020	Phantom 4 Pro	FC6310	P4P.20	65	5	1.9

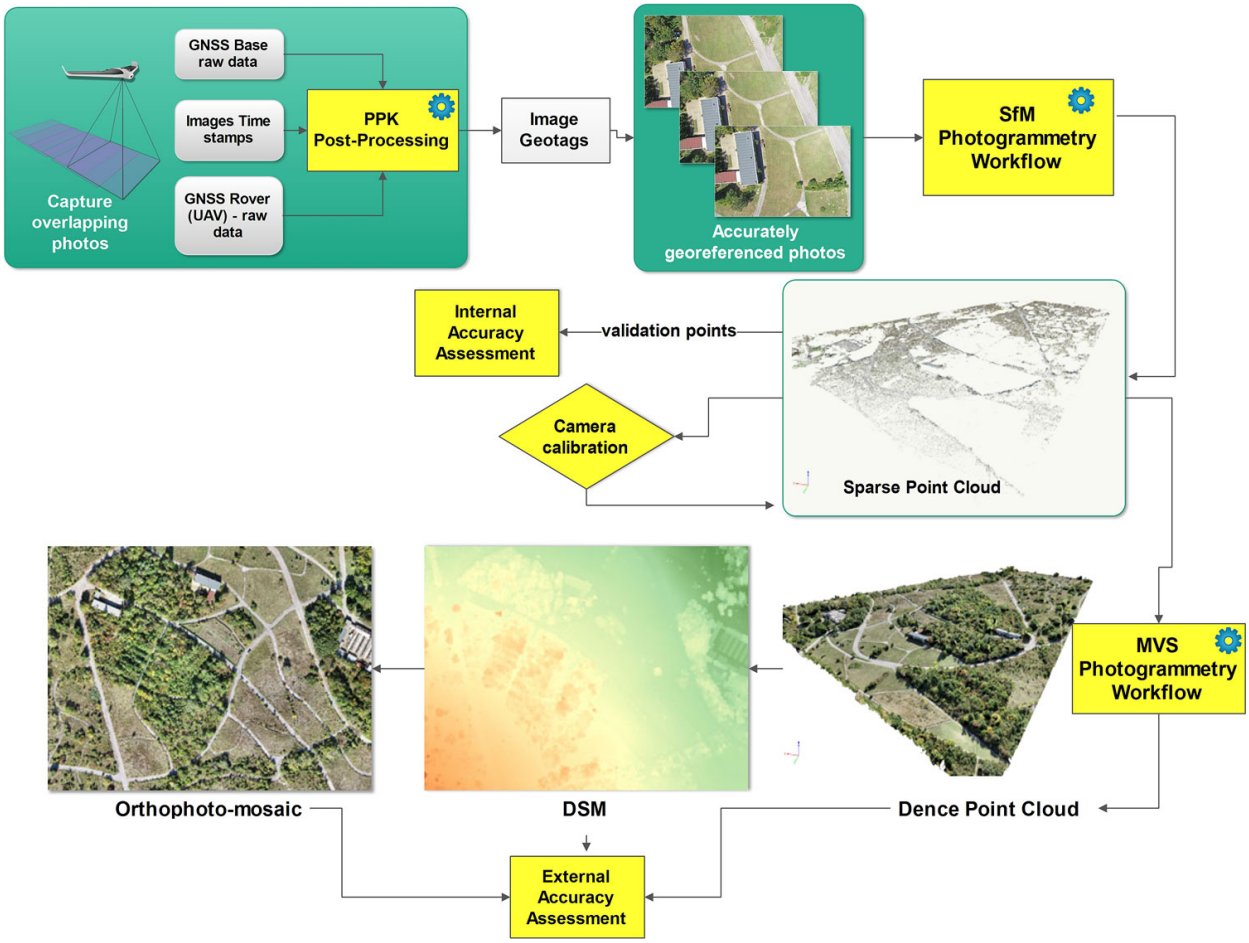

Figure 4. PPK-SfM-MVS workflow with accuracy assessment

As shown in (Fig. 4), the PPK-SfM-MVS process starts with initial data collection – photogrammetric surveying of the area and recording of GNSS raw data to implement PPK precision georeferencing of the images. The next step is the calculation of the precise coordinates of the photos after simultaneous processing of the GNSS records from the Rover (UAV) and the Base Station. Next is the application of the SfM method for calculating the camera parameters and generating an initial sparse cloud of points.

After this step, a first internal assessment of the accuracy of the initial model (via independent validation points) is performed, as well as an iterative calibration of the camera parameters. If we use GCP for precise model orientation, now is the time to input their coordinates and use them for georeferencing. After this computational stage is completed, processing continues through an MVS workflow to generate High-Resolution Topographic Data (HRTD): 1) Dense Point Cloud, 2) Digital Surface Model (DSM), and 3) Orthophoto Mosaic. The HRTD accuracy evaluation was performed outside the photogrammetry software to obtain an independent assessment of the final data.

2.4.2. GNSS measurements and PPK - image georeferencing

The control and validation points were coordinated by the GNSS RTK method with a geodetic dual-frequency receiver (Kolida - K5 PLUS). GCP and VP measurements were performed in RTK mode, receiving real-time coordinate corrections from 1YOCTO's CORS network. For a fixed solution, the declared accuracy of 1YOCTO is up to 5 cm.

The PPK method was applied to calculate the exact positions of the UAV images. A base station (GNSS BASE) was placed on the test site where the raw GNSS data was received and recorded by the EMLID RS+ receiver (Fig. 3b). During the UAV flight missions, the raw data and the timestamps of the photo acquisition were recorded using an additional Reach m+ single-frequency GNSS receiver mounted on the test UAVs.

The open-source software package RTKLib (Takasu and Yasuda 2009) was used to calculate the positions of the captured images through post-processing. The raw GNSS data from the UAV-mounted GNSS receivers, the raw data from the base station, and the image stamp file are input into RTKLib. Fixed solutions for the coordinates of photos were obtained by post-processing using RTKLib.

2.5. Photogrammetric processing and HRTD generation

Photogrammetric processing of the georeferenced images was performed with Pix4Dmapper (Pix4D S.A. 2022). The software uses the SfM-MVS algorithm to generate 3D point clouds, DSMs, and orthophoto mosaics from captured aerial photographs. When applying the PPK georeferencing method, the calculated camera positions are attached to the EXIF metadata of each captured image (Dinkov 2020). After initial processing, all validation points (Check points) are entered to assess accuracy. The following steps were generating a dense point cloud, orthophoto, and DSM to perform an independent evaluation outside the Pix4Dmapper photogrammetry software. The datasets were processed in nine combinations of the three air missions (Table 2) to evaluate the accuracy of the different georeferencing options.

2.6. Accuracy assessment

The most reliable assessment that can be made is based on the use of validation control points by measuring the differences between the HRTD (dense point cloud, orthophoto mosaic, and DSM) reported locations and the spatial coordinates measured in the field with a GNSS-RTK receiver. Accuracy evaluation of the point cloud, orthophoto mosaic, and DSM was performed using of 24 ground points (GCP and VP in different georeferencing configuration) (Fig. 5). For initial internal point cloud evaluation (SfM Photogrammetry Workflow), validation point positions are acquired directly into the 3D point cloud in Pix4D using the built-in RayCloud 3D Editor. The

Table 2. Flight mission configurations

Mission number	UAV	Camera	Georeferencing configurations:		
X6.20.1	Tarot X6	Sony A6000	9 GCP	PPK	PPK+1GCP
X6.20.2	Tarot X6	Sony RX0	9 GCP	PPK	PPK+1GCP
P4P.20	Phantom 4 Pro	FC6310	9 GCP	PPK	PPK+1GCP

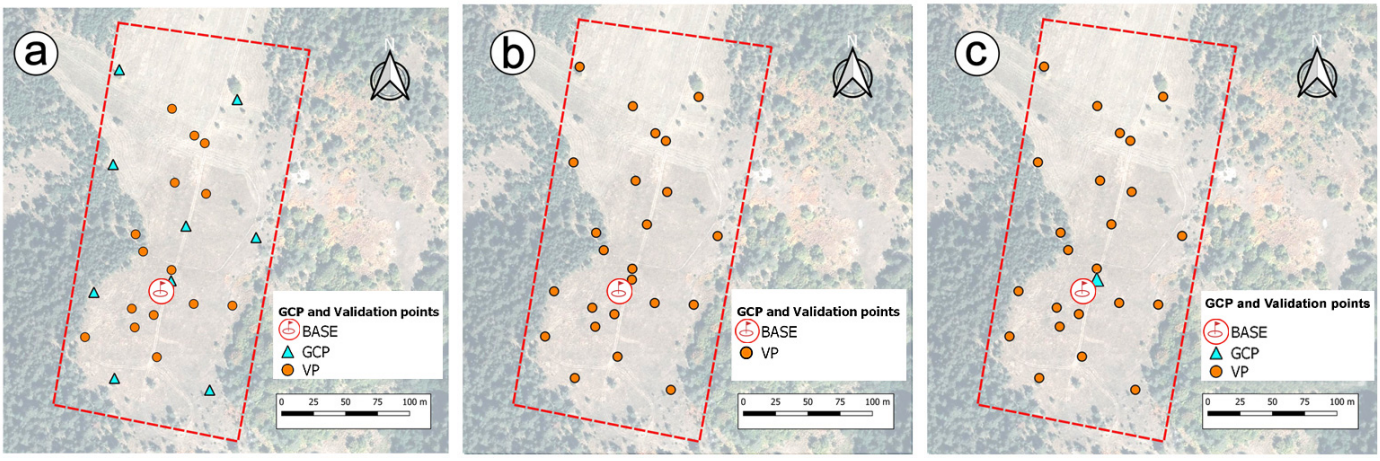

Figure 5. Distribution of GCPs and VPs and illustration of the different georeferencing configurations: (a) UAV onboard coordinate and indirect georeferencing by 9GCPs; (b) only PPK direct georeferencing; (c) PPK+1GCP georeferencing (one single control point was used)

point vectorization tool in the Pix4Dsurvey software was used to evaluate the accuracy of the generated dense point cloud externally. The vectorized points were exported as a point shapefile (.shp), and then processed in the open-source software QGIS (Team QGIS 2022). From QGIS, they are exported as text files with point Ids and X, Y, and Z coordinates. These coordinates are compared to the reference positions of the validation points. The accuracy of orthophoto mosaics and DSMs was evaluated using QGIS v.3.22.5 software. The X and Y coordinates of the validation points were obtained from identifying the centers of the targets in the orthophoto mosaic and recorded in a point shape layer. The DSMs and the "Point sampling tool" plugin were used to assign Z coordinates to the validation points. The points with their coordinates were exported as a text file and compared to their reference positions.

2.7.1. Statistical analysis

Calculation of root mean square errors (RMSE) in coordinates:

$$RMSE_x = \sqrt{\frac{\sum_{i=1}^{n} \Delta x_i^2}{n}} \quad (1)$$

$$RMSE_y = \sqrt{\frac{\sum_{i=1}^{n} \Delta y_i^2}{n}} \quad (2)$$

$$RMSE_z = \sqrt{\frac{\sum_{i=1}^{n} \Delta z_i^2}{n}} \quad (3)$$

Where Δxi, Δyi, and Δzi represent the differences between the reference coordinates and the HRTD (dense point cloud, orthophoto mosaic, or DSM) vectorized coordinates of the validation points, and *n* is the total number of validation points. RMSEx and RMSEy are used to calculate the root mean square error in the horizontal position RMSExy of the validation points:

$$RMSE_{xy} = \sqrt{RMSE_x{}^2 + RMSE_y{}^2} \quad (4)$$

3. Results

SfM-MVS image processing was performed with Pix4Dmapper software (Pix4D S.A., n.d.). Table 3 shows the initial parameters of the input data and the final parameters of the generated HRTDs.

3.1. Internal Accuracy Assessment using the Validation Points

The accuracy achieved in the validation points in the SfM-MVS photogrammetric processing software (Pix4DMapper 4.6.4) can be considered one of the earliest accuracy estimates during the workflow (Tomaštík et al. 2019). Validation point positions were acquired directly into the 3D point cloud in Pix4D using the built-in RayCloud 3D Editor. Horizontal and vertical root mean square errors of point positions for this type of estimation are reported in Tables 4 and 5.

Table 4. Horizontal root mean square errors in Position (RMSExy) of validation points used in Pix4Dmapper software (in meters).

Georeferencing method	**Configuration UAV/camera**		
	X6/A6000	X6/RX0	Phantom 4 Pro
9 GCP	0.025	0.028	0.026
PPK	0.125	0.180	0.231
PPK+1GCP	0.043	0.168	0.041

Table 5. Vertical root mean square errors (RMSEz) of validation points used in Pix4Dmapper software (in meters).

Georeferencing method	**Configuration UAV/camera**		
	X6/A6000	X6/RX0	Phantom 4 Pro
9 GCP	0.056	0.074	0.041
PPK	**1.968**	0.096	**2.502**
PPK+1GCP	0.053	0.092	0.051

Table 3. Topographic data with high-resolution - parameters

Configuration UAV/camera	**Average Ground Sampling Distance GSD (cm/pix)**	**Number of images**	**Dense Cloud** Number of 3D Densified Points / Average Density (per m³)	**DSM and Orthomosaic Resolution (cm/pix)**
TAROT X6/Sony A6000	1.56	112	77 452 317 2330.55/m³	3.12
TAROT X6/Sony RX0	2.38	112	43 314 820 558.62/m³	3.00
DJI Phantom 4 Pro	1.91	107	56 766 822 1107.81/m³	3.12

3.2. External Accuracy Assessment

3.2.1. Dense Point Cloud Accuracy

In the external evaluation of the generated dense point clouds (Fig. 6), there can hardly be a match between the coordinates acquired in the cloud and those measured by GNSS. In this case, using the closest possible point from the point cloud will generate up to additional identification errors. However, this error is usually small for well-modelled regions with a high density of cloud structure.

Horizontal and vertical root mean square errors of positions of points are reported in Tables 6 and 7.

A boxplots were used to graphically demonstrate the localization, spread, and skewness groups of reported errors by their quartiles. The horizontal line represents the median, the lower part of the hinge represents the 25th percentile, the upper part represents the 75th percentile, and whiskers represent 1.5 x IQR (inequality range) in both directions.

In Figures 7 and 8, the errors in the horizontal and vertical position of the validation points acquired in the dense point clouds are represented by boxplot diagrams.

Table 6. Horizontal root mean square errors in position (RMSExy) of validation points in the point cloud (in meters).

Georeferencing method	Configuration UAV/camera		
	X6/A6000	X6/RX0	Phantom 4 Pro
9 GCP	0.026	0.038	0.029
PPK+1GCP	0.046	0.158	0.068

Table 7. Vertical root mean square errors (RMSEz) for validation point positions in the point clouds (in meters)

Georeferencing method	Configuration UAV/camera		
	X6/A6000	X6/RX0	Phantom 4 Pro
9 GCP	0.061	0.066	0.052
PPK+1GCP	0.055	0.123	0.056

3.2.2. Orthomosaic and DSM Accuracy

The accuracy of the final raster photogrammetric products – ortho mosaics and DSM – was evaluated using the GIS software QGIS. First, the acquired X and Y planimetric coordinates of the validation points were output to an external point shapefile, where the points represent the centers of the landmarks recognized in the orthophoto mosaic. After this step, Z coordinates were added for the vectorized points, using an additional tool (plugin) to extract the Z values from the raster file (DSM). The coordinates' values thus obtained were exported as a text file and compared with the reference positions of the inspection points. The root mean square errors in the position acquired in the orthophoto mosaics and the vertical errors obtained in the DSMs are reported in Tables 8 and 9.

The distribution of planimetric errors in the validation points acquired in the orthophoto mosaics is reported in Fig. 9

Table 8. Horizontal root mean square errors in Position (RMSExy) for validation points orthomosaic (in meters).

Georeferencing method	Configuration UAV/camera		
	X6/A6000	X6/RX0	Phantom 4 Pro
9 GCP	0.035	0.037	0.040
PPK+1GCP	0.046	0.163	0.046

Table 9. Vertical root mean square errors (RMSEz) for validation point positions acquired on digital surface model (in meters)

Georeferencing method	Configuration UAV/camera		
	X6/A6000	X6/RX0	Phantom 4 Pro
9 GCP	0.046	0.068	0.060
PPK+1GCP	0.059	0.116	0.065

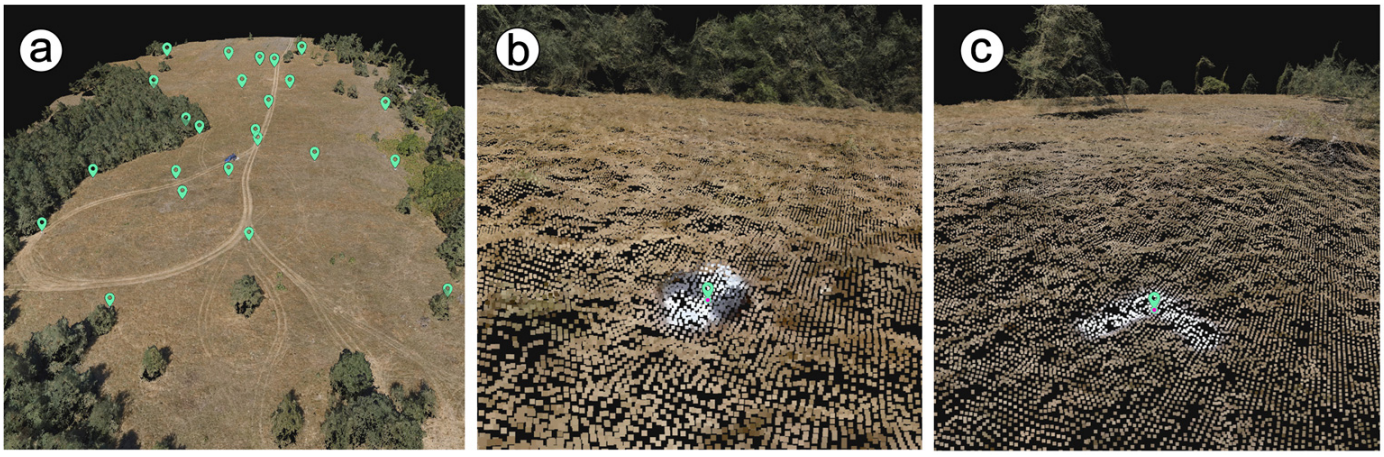

Figure 6. External evaluation of dense point cloud: (a) Dense cloud of test object - 3D view of validation points in Pix4DSurvey; (b), (c) Image of the ground marks in the dense point cloud and vector points on the targets.

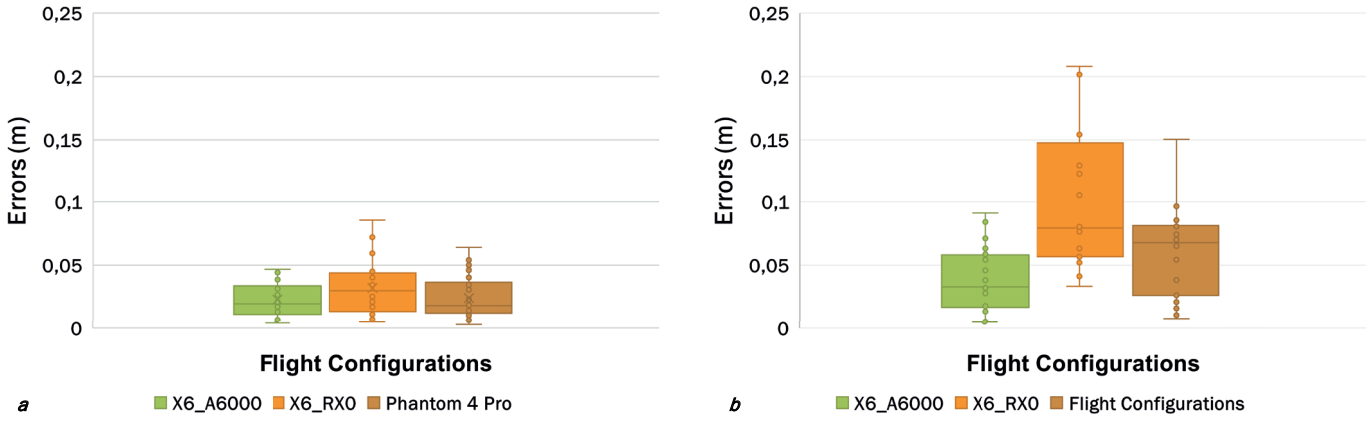

Figure 7. Boxplots for the errors in the horizontal position of the validation points acquired on the dense point clouds: (a) For indirect georeferencing through 9 GCP; (b) For direct PPK referencing with one control point (PPK +1 GCP).

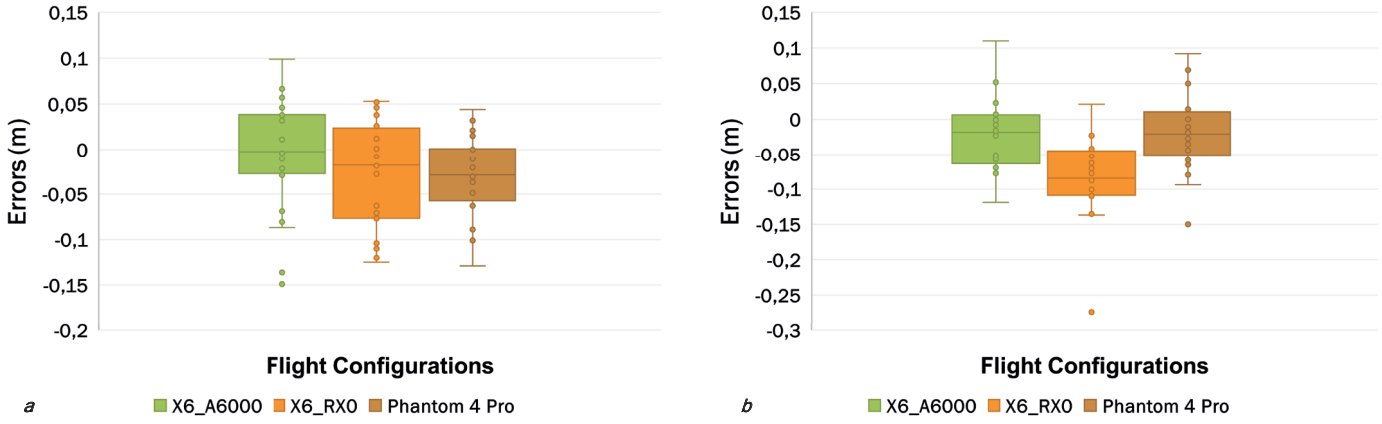

Figure 8. Boxplots for the errors in the vertical position of the validation points acquired on the dense point clouds: a) For indirect georeferencing through 9 GCP; (b) For direct PPK referencing with one control point (PPK +1 GCP).

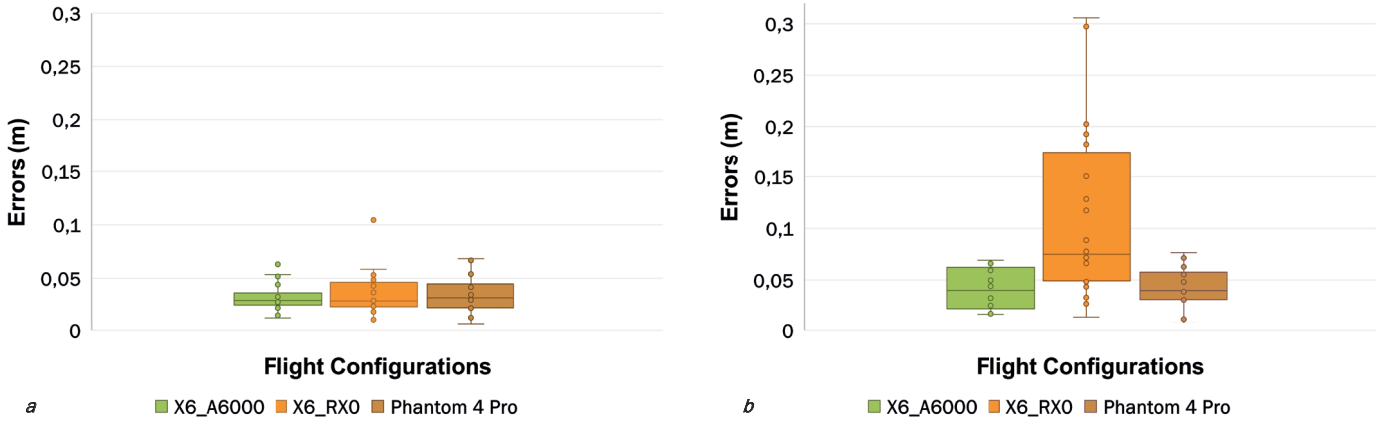

Figure 9. Boxplots for the errors in the horizontal position of the validation points acquired on the orthophoto mosaics: (a) For indirect georeferencing through 9 GCP; (b) For direct PPK referencing with one control point (PPK +1 GCP).

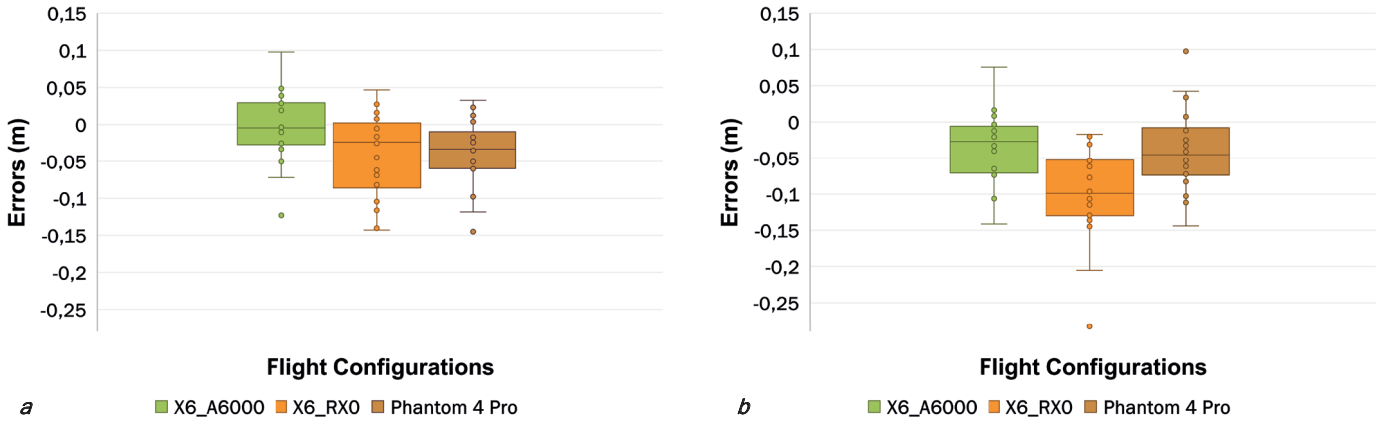

Figure 10. Boxplots for the errors in the vertical position of the validation points acquired on the terrain surface (DSM): (a) For indirect georeferencing through 9 GCP; (b) For direct PPK referencing with one control point (PPK +1 GCP).

4. Discusion

4.1. Interpretation of results

To evaluate and interpret the results, we will use the parameters developed in the ASPRS (American Society for Photogrammetry and Remote Sensing) Digital Geospatial Data Accuracy Standards (ASPRS 2014).

4.1.1. About the evaluation of the dense point cloud

- *Positional accuracy of the point cloud*

The root mean square error in position (RMSExy) of studied points from the generated dense point clouds, when applying the GCP method for georeferencing, is within 2.6-3.8 cm (about 1.6 GSD), which meets the requirements for "Standard mapping and GIS work" - table B.5 for scale 1:100 - table B.4 (ASPRS 2014). The PPK method with one GCP positional accuracy for X6/A6000 and P4P configurations are 4.6 and 6.8 cm (3.0-3.5 GSD GSD)), which meets the requirements for "Standart mapping and GIS work" - table B.5 for scale 1:200 - table B.4 (ASPRS 2014). In the X6/RX0 configuration, RMSExy is 15.8 cm or 6.6 GSD, which corresponds to the category "Visualization and less accurate work" table B.5 for scale 1:200 - table B.4 (ASPRS 2014).

- *Vertical accuracy of the point cloud*

According to the ASPRS accuracy standards (table B.7 (ASPRS 2014)), elevation data mainly have ten levels of accuracy associated with technologies such as mobile mapping systems, unmanned aerial systems, aerial or satellite imagery, Lidar, or IFSAR. In our research, the mean height accuracy (RMSEz) obtained in the dense point clouds, when applying the GCP georeferencing method, turns out to be within 5.2-6.1 cm, which corresponds to Vertical Accuracy Class 4 (10 cm). In the PPK method with one GCP, the vertical accuracy for the X6/A6000 and P4P configurations are similar (5.5-5.6 cm), and the digital data refer to the same Vertical Accuracy Class 4 (10 cm). In the X6/RX0 configuration, the RMSEz is 12.1 cm, corresponding to the next category Vertical Accuracy Class 5 (15) cm table B.7 (ASPRS 2014). The mean squared errors in position (Table 5) and in height (Table 6) are more significant than in the internal estimation of the point cloud. But the most likely reason is the difficulty matching the center of the target to the closest point of the 3D cloud (Fig. 6b, c).

- *Error in identifying the validation points in the dense cloud*

This error can significantly affect the results of the photogrammetric evaluation. The point identification process requires some operator experience with image interpretation. Although the points in our study were signalled using contrasting ground cues (Fig. 3), there were some difficulties during their identification in the cloud structures. The quality of the generated point cloud is particularly influential here. It can be seen from Table 3 that using a quality optical sensor (Sony A6000), we will get almost twice the number of points in the cloud, and its average density is three times bigger than the point cloud generated with an action camera. This circumstance affects the correct identification of the centers of the earth signs, which leads to greater accuracy of the surveyed position. As a confirmation of the hypothesis, in Figure 7. in the box-plot diagrams of point cloud errors, it can be seen that with the Tarot X6/A6000 configuration, we have the minor planimetric errors, which have the most compact distribution.

4.1.2. On the assessment of orthophoto mosaics

The root means square errors in the position of the orthophoto mosaics are analogous to the planimetric errors in the point clouds: 3.5-4.0 cm (about 1.6 GSD) for the GCP georeferencing method. In the PPK method with one GCP, the position accuracy for the X6/A6000 and P4P configurations is 4.6 cm (3.0 GSD), and for the X6/RX0 configuration, RMSExy is 16.3 cm or 6.8 GSD. Therefore, we classify orthophoto mosaics into the same planimetric accuracy categories according to (ASPRS 2014) as dense point clouds. This result was expected since point clouds are the primary product for HRTD generation.

4.1.3. Evaluation of DSMs

The average height accuracy of the raster surfaces (DSM) RMSEz, when applying the GCP method for georeferencing, is within 4.6-6.8 cm, which corresponds to Vertical Accuracy Class 4 (10 cm). Applying the PPK method with one GCP, the vertical accuracy for the X6/A6000 and P4P configurations are similar, 5.9-6.5 cm and the digital data is in the same Vertical Accuracy Class 4 (10 cm). With the X6/RX0 configuration, the vertical error RMSEz is 11.6 cm, which corresponds to the category of Vertical Accuracy Class 5 (15 cm) Table B.7 (ASPRS 2014).

4.2. PPK-SfM-MVS workflow with accuracy assessment

Evaluation of HRTD is an essential part of the workflow in producing quality digital data. Applying the "Internal Accuracy Assessment" in SfM-workflow gives an initial assessment of the accuracy of the input data. It is an essential step in camera calibration before proceeding to the next stage (MVS workflow) to generate the final dense point cloud, orthophoto mosaic, and DSM. The "External Accuracy Assessment" of the final digital products evaluates the accuracy of the acquired HRTDs and their quality for subsequent analysis and research. Applying the PPK-SfM-MVS workflow using (L1-GNSS) equipment provides close accuracy to traditional GCP georeferencing techniques but reduces significantly of fieldwork. This has also been found in other studies (Shouny et al. 2017) of the direct georeferencing method.

We evaluated digital data acquired with a budget-class UAV and single-frequency GNSS-PPK equipment. Various studies have evaluated accuracy with dual-frequency GNSS (L1/L2) through which ionospheric interference is reduced, as well as the resolution of phase cycle ambiguities, factors that make this system a faster, more accurate and more reliable alternative for positioning compared to single frequency GNSS (L1) (Ekaso et al. 2020).

No further processing was performed on the raw data to eliminate the tilt of the UAV in flight (Essel et al. 2022), synchronization between GNSS and cameras (Ekaso et al. 2020), or compensation for the delay in the time stamp from the Phantom 4 Pro LED when using the Tuffwing PPK-kit (Emlid. Community 2022). Our study shows the accuracies that can be achieved with such a class of systems without additional data processing and manipulation. With the UAV/camera configurations we tested, the required HRTD planimetric accuracies can be achieved subject to the following recommendations:

a) flight speed up to 5 m/s for the Phantom 4 Pro/ Tuffwing PPK configuration;
b) use of UAV flight planning and control software with terrain following option;
c) using a camera with appropriate performance: a mechanical shutter, a large sensor, and a lens with minimal distortion.

Following these recommendations, the accuracy of our final topographic data conforms to the category Standard Mapping, and GIS Work - table B.5 for a scale of 1:200 - table B.4 (ASPRS 2014).

The quality of the lens and sensor on the Sony RX0 action camera is reflected in the digital products' accuracy. Therefore, the assessment of the HRTD produced with this camera corresponds to the category "Visualization and less accurate work" table B.5 for scale 1:200 - table B.4 (ASPRS 2014) for planimetric accuracy and the category of Vertical Accuracy Class 5 (15 cm) table B.7 (ASPRS) for vertical accuracy.

5. Conclusion

This paper reports the results of evaluating the accuracy of high-resolution digital topographic data (HRTD) using direct georeferencing as a potential approach that can be applied to mapping and surveying non-urban areas. An empirical study was conducted to evaluate the accuracy of direct georeferencing using three budget configurations UAV, L1-GNSS, and camera.

The results highlight that the tested unmanned systems Phantom 4 Pro and Tarot X6 for photogrammetric aerial surveying of the test object with GSD 2-3 cm, EMLID single-frequency GNSS receivers, and Sony A6000, DJI FC6310 cameras through the applied PPK-SfM-MVS workflow provide the production of digital topographic products in the range "Standard mapping and GIS work" (M 1:200) (ASPRS 2014). Furthermore, based on the experimental tests, we conclude that the quality of the optical sensor significantly impacts the topographic products' accuracy, and the HRTD produced by the action camera Sony RX0 corresponds to the category "Visualization and less accurate work" (M 1:200) according to the standards of (ASPRS 2014).

The accuracy achieved using GCP for georeferencing is slightly better than the direct method achieved with the UAV/GNSS/camera systems tested in this study. Nevertheless, the indirect method requires a uniform and optimal spatial distribution of GCP in the study area (Stöcker et al. 2020). This makes surveying more labour-intensive and less efficient, especially for complex or dangerous terrain access cases. In such cases, using PPK solutions can significantly reduce field activities and costs, saving time and resources for placing GCP and geodetic measurements.

The main disadvantage of the single-frequency GNSS onboard receivers used in our workflow is the systematic height errors, which are easily solved using one ground control point.

Funding program

This study has been accomplished in the research project "Post-processing kinematic method for precise georeferencing of unmanned aerial vehicle images for 4D modeling of the earth's surface", № KP-06-M34/2 , National Science Fund (2019-2021).

Acknowledgements

The author would like to thank Atanas Kitev (NIGGG-BAS) for his help and effort in technical support in UAV systems and fieldwork.

References

ASPRS (American Society for Photogrammetry and Remote Sensing) (2014) ASPRS Positional Accuracy Standards for Digital Geospatial Data. Photogrammetric Engineering & Remote Sensing 1 (1): 1-26. https://www.asprs.org/wp-content/uploads/2015/01/ASPRS_Positional_Accuracy_Standards_Edition1_Version100_November2014.pdf

Dinkov D (2020) Applicability Of Open Source Unmanned Aerial System (UAS) For Photogrammetric Capturing And Mapping Of The Earth's Surface. XXX International Symposium on Modern Technologies, Education and Professional Practice in Geodesy and Related Fields, Sofia (Bulgaria), November 2020. FNTS.

Dinkov D (2021) Geospatial point clouds generated form images taken with unmanned aerial systems and applied direkt (PPK) method for georeferencing: Assessment of accuracy for a test area in the Plana mountain, Bulgaria. XXXI International Symposium on Modern Technologies, Education and Professional Practice in Geodesy and Related Fields, Sofia (Bulgaria), November 2021, 118-131.

Duró G, Crosato A, Uijttewaal WSJ, Kleinhans MG (2018) Monitoring Bank Erosion with Unmanned Aerial Vehicle (UAV) During a Low-water Event. 4TU.ResearchData. https://doi.org/10.4121/uuid:4eab4339-52d6-4328-81b2-640544c05438

Ekaso D, Nex F, Kerle N (2020) Accuracy assessment of real-time kinematics (RTK) measurements on unmanned aerial vehicles (UAV) for direct geo-referencing. Geo-spatial Information Science 23 (2): 165-181. https://doi.org/10.1080/10095020.2019.1710437

Eltner A, Kaiser A, Castillo C, Rock G, Neugirg F (2016) Image-based surface reconstruction in geomorphometry – merits, limits and developments. Earth Surface Dynamics. https://doi.org/10.5194/esurf-4-359-2016

Emlid. Community (2022) Reach M / Tuffwing PPK kit / RS2 Base / P4PV2 PPK Issues. https://community.emlid.com/ - Emlid Tech Kft, January 22. https://community.emlid.com/t/reach-m-tuffwing-ppk-kit-rs2-base-p4pv2-ppk-issues/28979

Essel B, McDonald J, Bolger M, Cahalane C (2022) INITIAL STUDY ASSESSING THE SUITABILITY OF DRONES WITH LOW-COST GNSS AND IMU FOR MAPPING OVER FEATURELESS TERRAIN USING DIRECT GEOREFERENCING. Int. Arch. Photogramm. Remote Sens. Spatial Inf. Sci. (Copernicus Publications), XLIII-B2-2022: 37-44. https://doi.org/10.5194/isprs-archives-XLIII-B2-2022-37-2022

Fazeli H, Samadzadegan F, Dadrasjavan F (2016) EVALUATING THE POTENTIAL OF RTK-UAV FOR AUTOMATIC POINT CLOUD GENERATION IN 3D RAPID MAPPING, Int. Arch. Photogramm. Remote Sens. Spatial Inf. Sci., XLI-B6: 221–226. https://doi.org/10.5194/isprs-archives-XLI-B6-221-2016

Fonstad MA, Dietrich JT, Courville BC, Jensen JL, Carbonneau PE (2013) Topographic structure from motion: a new development in photogrammetric measurement. Earth Surf. Process. Landforms, 38: 421-430. https://doi.org/10.1002/esp.3366

Forlani G, Dall'Asta E, Diotri F, Cella UMd, Roncella R, Santise M (2018) Quality Assessment of DSMs Produced from UAV Flights Georeferenced with On-Board RTK Positioning. Remote Sensing 10 (2): 311. https://doi.org/10.3390/rs10020311

Furukawa Y, Hernández C (2015) Multi-View Stereo: A Tutorial. Foundations and Trends® in Computer Graphics and Vision 9(1-2): 1-148. http://dx.doi.org/10.1561/0600000052

Harwin S, Lucieer A (2012) Assessing the Accuracy of Georeferenced Point Clouds Produced via Multi-View Stereopsis from Unmanned Aerial Vehicle (UAV) Imagery. Remote Sensing 4: 1573-1599. https://doi.org/10.3390/rs4061573

Jovančević SD, Peranić J, Ružić I et al. (2016) Analysis of a historical landslide in the Rječina River Valley, Croatia. Geoenviron Disasters 3: 26. https://doi.org/10.1186/s40677-016-0061-x

Pix4D S.A. n.d. (2022) pix4d.com. Pix4D S.A. Accessed 09 8, 2022 https://www.pix4d.com/product/pix4dmapper-photogrammetry-software

Sanz-Ablanedo E, Chandler JH, Rodríguez-Pérez JR, Ordóñez C (2018) Accuracy of Unmanned Aerial Vehicle (UAV) and SfM Photogrammetry Survey as a Function of the Number and Location of Ground Control Points Used. Remote Sensing 10 (10): 1606. https://doi.org/10.3390/rs10101606

Shouny AE, Yakoub N, Hosny M (2017) Evaluating the Performance of Using PPK-GPS Technique in Producing Topographic Contour Map. Marine Geodesy 40 (4): 224-238. https://doi.org/10.1080/01490419.2017.1321594

SPH Engineering (2022) UgCS. 12 10. Accessed 10 10, 2022. https://www.ugcs.com/.

Smith MW, Carrivick JL, Quincey DJ (2016) Structure from motion photogrammetry in physical geography. Progress in Physical Geography: Earth and Environment 40 (2): 247-275. https://dx.doi.org/10.1177/0309133315615805

Stöcker C, Nex F, Koeva M, Gerke M (2017) Quality assessment of combined IMU/GNSS data for direct georeferencing in the context of UAV-based mapping. The International Archives of the Photogrammetry, Remote Sensing and Spatial Information Sciences, Bonn (Germany), XLII-2/W6: 355–361. https://doi.org/10.5194/isprs-archives-XLII-2-W6-355-2017

Stöcker C, Nex F, Koeva M, Gerke M (2020) High-Quality UAV-Based Orthophotos for Cadastral Mapping: Guidance for Optimal Flight Configurations. Remote Sensing 12 (21): 3625. https://doi.org/10.3390/rs12213625

Takasu T, Yasuda A (2009) Development of the low-cost RTK-GPS receiver with an open source program package RTKLIB. International Symposium on GPS/GNSS. Jeju, Korea.

Team QGIS, Development (2022) A Free and Open Source Geographic Information System. Open Source Geospatial Foundation. Accessed 10 10, 2022. https://www.qgis.org/en/site/index.html

Tomaštík J, Mokroš M, Surový P, Grznárová A, Merganič J (2019) UAV RTK/PPK Method—An Optimal Solution for Mapping Inaccessible Forested Areas? Remote Sensing 11 (6): 721. https://doi.org/10.3390/rs11060721

Turner IL, Harley M, Drummond C (2016) UAVs for coastal surveying. Coastal Engineering (114): 19-24. https://doi.org/10.1016/j.coastaleng.2016.03.011

Zhang H, Aldana-Jague E, Clapuy F, Wilken F, Vanacker V (2019) Evaluating the potential of post-processing kinematic (PPK) georeferencing for UAV-based structure-from-motion (SfM) photogrammetry and surface change detection. Earth Surface Dynamics 7: 807–827. https://doi.org/10.5194/esurf-7-807-2019

Conflict of interest

The authors have declared that no competing interests exist.

ORCID

https://orcid.org/0000-0001-5592-636X - D. Dinkov